Springer

Journal of
Mechanical
Science and
Technology

Journal of Mechanical Science and Technology 22 (2008) 1154~1162

www.springerlink.com/content/1738-494x

A comparison of LII analysis results from numerical model and experiment at elevated surrounding pressures

Gyu Bo Kim[1], Jae Young Shim[1], Seung Wan Cho[1], Young June Chang[2] and Chung Hwan Jeon[2,*]

[1]*Graduate School of Mechanical Engineering, Pusan National University, 30 San Jangjeon-dong, Geumjeong-gu, Busan 609-735, South Korea*

[2]*School of Mechanical Engineering, RIMT, Pusan Clean Coal Center, Pusan National University, 30 San Jangjeon-dong, Geumjeong-gu, Busan 609-735, South Korea*

(Manuscript Received February 8, 2007; Revised November 30, 2007; Accepted January 26, 2008)

Abstract

With environmental concerns over emitted particulate matters(PM) from combustion systems, various researches have been conducted on reduction and measurement techniques of particulate matters. The LII analysis results from numerical models and experiments in an ethylene/air laminar diffusion flame at elevated pressure up to 2.0 MPa with laser fluence 0.07 J/cm^2, detection wavelength 400 nm were compared to validate a modified LII numerical model. The lifetime of the LII signal decreased as the elevated pressure increased, so that LII decay time also decreased in both results. In the aspect of heat transfer mechanism, it becomes earlier that dominant conduction starts. This shows that the results matched well under the pressure conditions. It is concluded that the LII numerical model could be applied to decide particle size in TIRE-LII at the high-pressure condition.

Keywords: Laser induced incandescence; Particulate matters; Primary particle size; Decay time; Surround pressure

1. Introduction

With the awareness of the serious effects caused by emissions from combustion systems, such as vehicle engines, power generation facilities and furnaces, many countries have tightened regulations on environmental pollution.

Emissions from combustion systems consist of many different kinds of matters such as NOx, CO_2, HC, particulate matters and so on. These emissions have caused greenhouse effect which leads to changes in the Earth's climate, acid rain, and health problems such as several pulmonary diseases [1].

Specially, it is known that particulate matters (PM) are very harmful in causing pulmonary carcinoma. So, PM, commonly called soot, is the one of the spotlighted research topics among researchers. Many researchers who have studied soot were concerned about the soot volume fraction rather than PM size in the 1990s.

But, Suntz and Bockhorn presented that the toxicity of soot emitted from combustion applications is associated with the soot particle size distribution rather than with the total mass of soot. Later, environmental regulations introduced PM size instead of soot volume fraction [2].

There are several methods for measurement of soot. It is classified mainly into two categories: intrusive and non-intrusive. Non-intrusive methods such as optical soot diagnostics are currently in the spotlight. Among several optical soot diagnostics, it is known that laser- induced incandescence (LII) is the most powerful method because it can measure soot particle size, soot volume fraction mass faction etc. simultaneously. It is also preferred in many combustion sys-

*Corresponding author. Tel.: +82 51 510 3051, Fax.: +82 51 582 9818
E-mail address: chjeon@pusan.ac.kr
DOI 10.1007/s12206-008-0120-7

tems because it is capable of *in-situ* measurement and high temporal, spatial resolution. Time-resolved laser-induced incandescence (TIRE-LII) is the one of the applied LII techniques to measure a primary soot particle size by calculating the signal ratio at two different signal detection times.

The earliest evidence of the LII technique was in an observation of the different temporal emission profiles of different-sized particles in laser-irradiated carbon black and aerosols by Week and Duley in 1974 [3]. This laser-induced optical signal was first found as interference during Raman measurements in a flame by Eckbreth in 1977 [4]. The observation and analysis modeling in that research are the starting point and first thorough resource for most LII investigations these days.

The first effort to model the nano-scale energy and mass transfer processes of soot in LII was made by Eckbreth. Melton performed numerical calculations to investigate the possibility of developing a soot diagnostic based on the laser heating of particles. Melton concluded that LII might be possible to obtain the particle temperature, soot primary particle size distribution parameters, and relative soot volume fraction [5]. On the other hand, Dasch experimentally and numerically examined the particle vaporization induced by high intensity laser pulses, and concluded that vaporization will occur at the surface and the particle size will shrink inwards [6].

Quay et al. revealed that the LII signal has linearity with the laser fluence, and there is a plateau region in the excitation curve over the certain laser fluence [7]. Will et al. proposed that TIRE-LII be used to measure primary soot particle size by signal ratio with temporal behavior of LII signal using a two-dimensional imaging technique in the flame [8]. Hofmann performed an experiment to discuss the implications for primary soot particle size and soot volume fraction at elevated pressure [9].

Recently, Schultz et al. compared the model implications made by many LII research groups to adjust and provide the best choice of the model. According to Schultz, there is no perfect LII model because there are still many unknown optical properties and many uncertainties in the model [10].

An objective of this research is to validate a modified LII numerical model through the comparison of results obtained from an experiment under elevated surrounding pressure. For the evaluation of the validity of the LII numerical model, vaporization, conduction, radiation, LII signal, soot particle temperature, change of primary particles size, decay time are considered in comparison.

2. Modeling of laser-induced incandescence

2.1 Heat and mass transfer model

Laser-induced incandescence technique is based on the fact that soot particles absorb the laser light and reach, during the laser pulse, well above vaporization temperature of soot [11]. The radiation of the heated particles is then time resolved detected during the cooling phase. Soot particles are assumed as a single primary particle in point contact and monodispersely distributed to analyze LII signal and primary soot particles by a numerical model. A schematic representation of the power balance of LII is shown in Fig. 1.

The particle heating is described by an absorption term. The cooling of the particles is mainly due to vaporization of the particles, heat conduction and conduction to the surrounding gas, and blackbody radiation of energy [12].

The general rate equation that describes the energy balance for the interaction of a particle with light is given by

$$\frac{dU}{dt} = \dot{Q}_{abs} - \dot{Q}_{vap} - \dot{Q}_{con} - \dot{Q}_{rad} \tag{1}$$

The left side term dU/dt describes the internal energy of the particles. Soot particles are heated up by absorbed laser intensity $I_L(t, x)$ and the absorption term Q_{abs} can be described as a function of projected particle area and absorption coefficient $\alpha_{abs}(r, \lambda_0)$ of the particle at wavelength λ_0, which is calculated

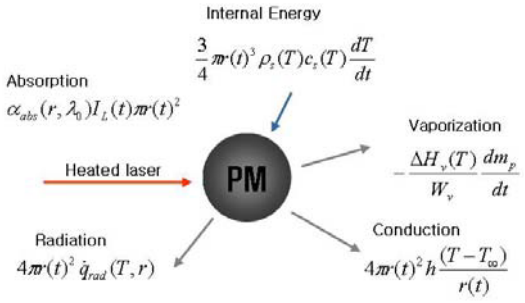

Fig. 1. Schematic presentation of power balance of a laser heated soot particle.

from a model for Mie scattering of spherical particles [12].

The vaporization term takes the temporal change of mass. W_v is the molecular weight of the soot vapor. $\Delta H_V(T)$ represents the enthalpy of vaporization. The molecular weight of the soot vapor and the enthalpy of vaporization are obtained from the equilibrium calculations of Leider et al. and expressed as a fifth-order polynomial expression [13].

Heat loss due to conduction is determined by the particle surface area and the temperature difference with respect to the surrounding gas temperature T_∞ and heat transfer coefficient h.

An estimation of heat transfer coefficient h, given by McCoy et al. depends on a geometry heat transfer factor G and the Knudsen number Kn [14]. The mean free path of the soot particles in air λ_{mfp} is calculated from a Sutherlands approximation for the dynamic viscosity of air [15]. The detected Planck radiation is one of the main paths of heat loss. q_{rad} denotes the radiation term and it is calculated by an integral over the emission wavelengths. The particle emissivity is assumed to be equal to its absorption coefficient $\alpha_{abs}(r,\lambda)$.

The overall energy balance equation, non-linear differential equation for the particle temperature T can be deduced as

$$\frac{dT}{dt} = -\frac{3\dot{q}_{rad}(T,r)}{r(t)\rho_s c_s} - \frac{3(T-T_\infty)k_\infty}{[1+G\lambda_{mfp}/2r(t)]r(t)^2\rho_s c_s} + \frac{3\alpha_{abs}(r,\lambda_0)I_L(t,x)}{4r(t)\rho_s c_s} + \frac{3\Delta H_V(T)r(t)}{W_V r(t)c_s} \quad (2)$$

The mass balance is the soot particles is given by

$$-\rho_s \frac{dr}{dt} = \rho_V U_V \quad (3)$$

where ρ_s is the density of the solid soot particle, which is dependent on the particle temperature, ρ_V is the density of vaporized soot and U_v is the Langmuir evaporation rate. ρ_V and U_v are calculated from the Clausius-Clapeyron equation with an assumption of an ideal gas. [15]

The overall mass balance equation, non-linear differential equation for the soot particle radius r can be deduced as

$$\frac{dr}{dt} = -\frac{p^*}{\rho_S}\sqrt{\frac{W_V}{2R_m T}}\exp\left[\frac{\Delta H_V(T)(T-T^*)}{R_m T T^*}\right] \quad (4)$$

2.2 Thermodynamic properties of soot

To achieve more accurate LII signal information, it is necessary to apply thermodynamic properties of soot, which are a function of soot particle temperature into the model. There are mainly five thermodynamic properties of soot, which influence and affect the LII signal in the model and a function of soot particle temperature based on our knowledge.

A detailed description and mathematical expression of thermodynamic properties of soot are explained below.

To account for changes in the particle density and specific heat with temperature, the model incorporates formulations for these parameters given by Fried and Howard for solid graphite [16]. Linear fits to the formulations from Fried and Howard for solid graphite density yield

$$\rho_s = 2.3031 - 7.3106\times10^{-5}T \quad (5)$$

The equation given in Fried and Howard for the specific heat of solid graphite is

$$c_s = \left(\frac{R}{12.01}\right)\{1.115\left(\frac{597}{T}\right)^2\exp\left(\frac{597}{T}\right)\left[\exp\left(\frac{597}{T}\right)-1\right]^{-2} + 1.789\left(\frac{1739}{T}\right)\exp\left(\frac{1739}{T}\right)\left[\exp\left(\frac{1739}{T}\right)-1\right]^{-2} + 1.16T\} \quad (6)$$

The parameters in the vaporization term, the vaporized molecular weight W_V, the heat of vaporization $\Delta H_V(T)$, and vaporized pressure of soot P_V are particle temperature dependent. These properties are obtained form the equilibrium calculations of Leider et al. and given as a fifth-order polynomial expression [13].

$$W_V = \sum_{i=0}^{5} w_i T^i \quad (7)$$

$$\Delta H_V = \sum_{i=0}^{5} h_i T^i \quad (8)$$

$$P_V = \exp\left(\sum_{i=0}^{5} p_i T\right) \quad (9)$$

2.3 LII signal

The LII signal can be directly performed on the basis of particle size and the calculated temperature. The following LII signal is proposed by Will :

$$S_{LII} \propto r^2 \int R(\lambda)\alpha_{abs}(r,\lambda)\frac{c_1 {n_\infty}^2}{\lambda^5(e^{c_2/\lambda T}-1)}d\lambda \qquad (10)$$

$R(\lambda)$ is a combined spectral response function, which takes into account the sensitivity of the detector and the transmission of the optical system [17].

2.4 LII signal decay rate

Primary particle size is deduced from TIRE-LII technique to calculate decay rate at two different signal detection times. LII signal decay time τ, which is a function of primary particle size, can also offer primary particle information such as primary particle size with assumption that the LII signal is represented as the following expression [18, 19].

$$S(t_2) \propto S(t_1)\exp\left(-\frac{t}{\tau(r)}\right) \qquad (11)$$

3. Experimental apparatus and method

In this experiment, a high-pressure combustion chamber (ILSHIN AUTOCLAVE Co., Ltd.) made for working pressure conditions up to 10MPa at 500 K is used. The chamber consists of three parts: exhaust pressure control parts for elevating or holding pressure conditions, optical access parts to measure as three axial directions into the chamber, and combustor parts for forming laminar diffusion flame. A schematic diagram of the chamber is shown in Fig. 2. The diameter of the chamber is set to 150mm and the height of the chamber is 200mm. It is built for a laminar diffusion flame burner with fuel tube(ϕ = 2.29mm) and surround air tube(ϕ = 25.4mm). A chimney is set to prevent effects of the recirculation gas above the burner tip.

To improve flame stability, a tapered fuel tube and a chimney with four quartz plates of a square tube is used.

Ethylene is used as the fuel supply for elevated pressure conditions. Then for fuel and air flow rate we used a metering valve to maintain flow rates and flame stability for high pressure. Flame height is about 10mm at elevated pressure conditions 0.1 to 0.5MPa and 7mm at 1.0 and 2.0MPa. LII signals are detected at the center of the flame for radial direction as following flame heights. In this study, characteristics of LII signals are analyzed by comparing detected LII signals with numerical results of the LII model.

The optical measurement system for LII is as follows: pulsed Nd:YAG laser (λ_{2nd} = 532nm, 9ns FWHM, 10Hz) as heating source of particulate matters, photo multiplier tube, 400 ± 10 nm narrow bandpath filter for collecting LII signal, oscilloscope (500Mhz, 1Gs/s) for analyzing LII signal. A schematic diagram of the system is shown in Fig. 3.

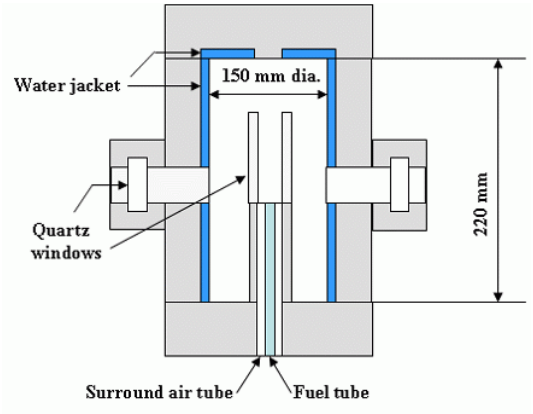

Fig. 2. Schematic of the high pressure combustion chamber.

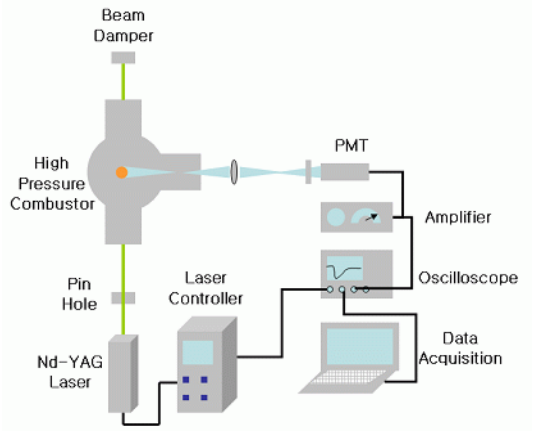

Fig. 3. Schematic of measurement system for laser induced incandescence.

4. Result and discussion

4.1 Heat transfer mechanism

The heat transfer mechanism was investigated to figure out which heat transfer mechanism was the most dominant factor that affects the LII signal, soot temperature and soot particle size. Numerical study was carried out at the given conditions: laser fluence is 0.07 J/cm^2, soot particle size is 30 nm, surround gas temperature is 1800 K and pressures are 0.1 MPa and 0.5MPa. Fig. 4 shows the numerically calculated heat transfer mechanism of LII, which shows vaporization, conduction and thermal radiation.

From Fig. 4(a), it can be seen that the vaporization term is the dominant mechanism for some 170 ns and that afterward the conduction term determines the signal decay of the LII signal. Particle cooling process by LII signal decay can be described through the heat transfer mechanism. It is possible to measure soot particle size theoretically by analyzing the heat transfer mechanism using TIRE-LII. The conduction term is the most valuable term to measure soot particle size by using the LII signal ratio in TIRE-LII, which means that particle size can be determined by LII signal ratio after 170 ns on TIRE-LII.

Fig. 4(b) shows the heat transfer mechanism of LII when pressure is set to 0.5 MPa. The conduction term is the most dominant factor in the whole period compared to Fig. 4(a). In high pressure conditions, particle size can be determined by LII signal ratio after about 23 ns with a linear section on TIRE-LII.

4.2 Effects of elevated surrounding pressure on LII signal

The temporal behavior of the LII signal, particle temperature and particle size at elevated surrounding pressures up to 2.0 MPa was investigated through this study.

Fig. 5 shows characteristics of the LII signal at elevated pressure conditions. The signals are normalized to their maximum value for examining the difference of the signal decay equal to particle size with various surrounding pressures. As shown, the signal decay is steeper and lifetime of signal is shortened as surrounding pressure increases. This means that the soot particle temperature of one which has a high surrounding pressure cools down faster than one which has a low surrounding pressure because the dominant heat transfer at most of the period is conduction. Especially, the lifetime of LII signals is shortened, which means that it is hard to apply TIRE-LII at high-pressure conditions. Therefore, it is necessary to resolve time earlier than about 50ns on TIRE-LII at high-pressure conditions.

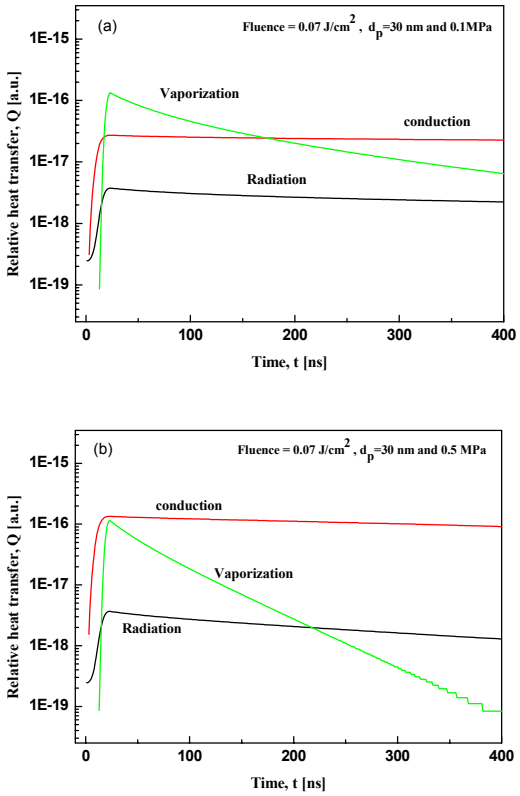

Fig. 4. Heat transfer mechanism of LII at given conditions: fluence is set to 0.07 J/cm^2, soot particle size is 30 nm and elevated pressure conditions are 0.1 MPa (a) and 0.5 MPa (b).

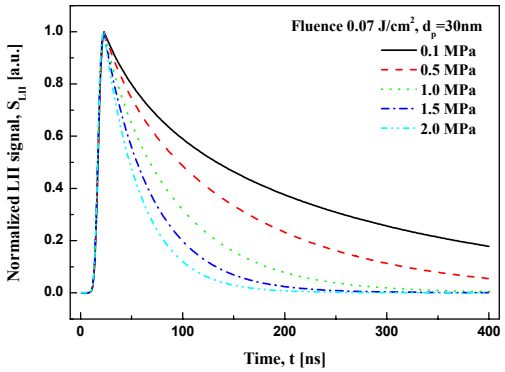

Fig. 5. Normalized LII signal as elevated surrounding pressure up to 2.0 MPa as numerical results.

Particle temperatures as elevating surrounding pressures up to 2.0MPa are depicted in Fig. 6. As can be seen in Fig. 6, soot particle temperature steeply decreases as surrounding pressure increases. The main reason of steep soot particle temperature decrease is that soot particles in high-pressure conditions have a higher conduction effect on cooling behavior. In the conduction equation of the energy balance as shown previously, the mean free path decreases with increasing surrounding pressure. With increasing The heat transfer coefficient in the conduction term increases with decreasing Knudsen number. Due to increase of heat transfer coefficient in the conduction term, the particle temperature decreases at high pressure. Namely, particles are cooled at high-pressure conditions faster than at ambient pressure conditions.

Fig. 7 shows characteristics of heated particle size by absorbed energy at elevated surrounding pressures up to 2.0MPa. In the case of 0.1MPa, the vaporization term is the dominant mechanism at the early stage and in the case of the others the conduction term dominates heat transfer mechanism for most of the period, so a great change of particle size at 0.1MPa is induced by the vaporization term and less change of particle size is induced. The reason might be that conduction term is more dominant than the vaporization term in the heat transfer mechanism as surrounding pressure increases. Additionally, LII signal decay with larger diameter is slower than the signal with smaller diameter. Since smaller soot cools down faster and diminishes faster, the LII signal of smaller diameter decreases steeply. The soot temperature decay has almost the same tendency as the LII signal shown in Fig. 6. In the relevant soot particles, it is found that larger soot particles attain slightly higher temperature during the laser pulse and that these cool down slower due to a smaller specific surface area.

Fig. 8 shows decay times, τ, of calculated LII signals at each surrounding pressure condition. Signal decay time as a function of soot particle size is determined by calculation of two signals ratio at two different times, which are based on dominant conduction as one of the heat transfer mechanisms. In the case of 0.1MPa, two different times selected 200 ns and 400 ns from pumped start point of laser energy and selected 50ns and 100ns at high pressure conditions.

Overall, decay time relatively linearly increases as particle size increases and decreases with elevated surrounding pressure. The slope of decay time as surrounding pressure increases more is slow. From this result, it is considered that the slope of decay time

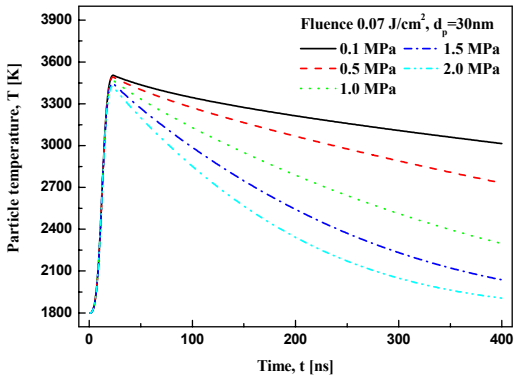

Fig. 6. Particle temperature at elevated surrounding pressures up to 2.0MPa as numerical results.

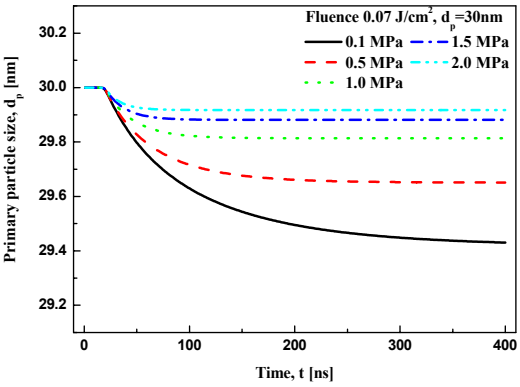

Fig. 7. Characteristics of heated particle size by absorp- tion energy as numerical results.

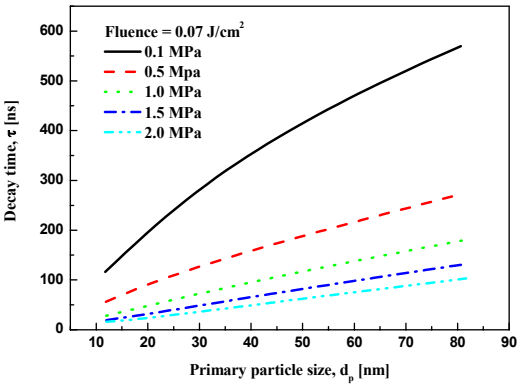

Fig. 8. Signal decay time at elevated surrounding pressure up to 2.0MPa as numerical results.

will be nearly zero if pressure condition is higher than 2.0 MPa. It means that measurement of particle size may be impossible by TIRE-LII at higher-pressure conditions anymore.

Experimental results for the simplified normalized LII signal at elevated surrounding pressure up to 2.0 MPa are depicted in Fig. 9. Experimental conditions follow as: laser fluence is 0.07 J/cm^2, detection wavelength is 400 $\pm$ 10 nm and surrounding pressure conditions are from 0.1 up to 2.0 MPa. The measured LII signal fluctuated little and LII signal was simplified throughout moving average process with 20 points of detected data. Each LII signal is detected at center of radial direction of flame and as axial direction of flame height above burner tip. Particle size on LII signal is unknown until comparing the detected signal with numerical results.

And then it cannot accurately compare measured data with numerical results, but a trend may be possible.

As shown in Fig. 9, the lifetime of the LII signal decreases as surrounding pressure increases. In case of 0.1 MPa, the lifetime of the signal was maintained about 1000 ns, but the lifetime of the signal was decreased about 350 ns in the case of 2.0 MPa. These trends are similar to numerical results for the lifetime of LII signal as surrounding pressure increases.

Especially, in case of 0.5 MPa, the lifetime of the LII signal was maintained over one of 0.1 MPa. This trend is different from numerical results. Due to this, it is necessary to investigate the LII model at high-pressure conditions.

LII signal decay is steeper as surrounding pressure increases, except the case of 0.5 MPa. This means that the soot particle temperature at low surrounding pressure cools down faster than soot which has high surrounding pressure because the dominant heat transfer is conduction mechanism.

Fig. 10 shows a comparison of signal decay with experimental and predicted results for signal decay times. From this result, it is postulated that the decay time of LII signal decreases with increasing elevated pressure. Additionally, there is no relationship between the decay time and the soot particle size in this case.

Especially, in the case of 0.1 MPa, particle size was elevated less than 20nm of predicted size. It is thought that will be necessary to divide a pressure condition at some phase because the LII model with considering pressure cannot probably satisfy the condition against low pressure condition.

Fig. 11 shows normalized LII signals at surrounding pressure 1.5 MPa. Normalized LII signals were compared for the experimental result and the pre-

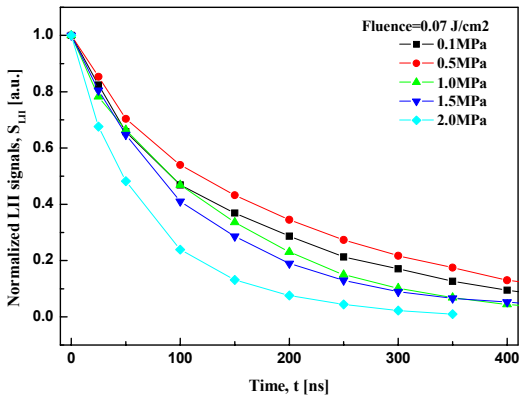

Fig. 9. Normalized LII signal at elevated surrounding pressures as experimental results: The signals are normalized to their maximum.

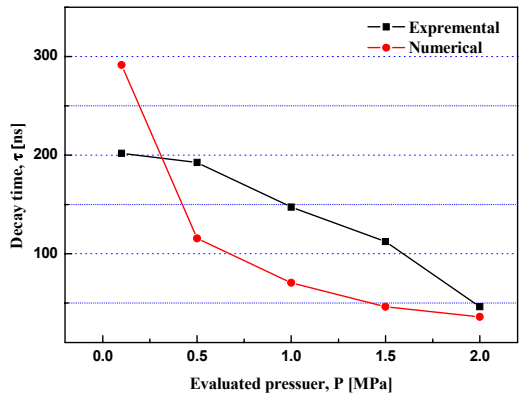

Fig. 10. Comparison of signal decay times as elevated surrounding pressure.

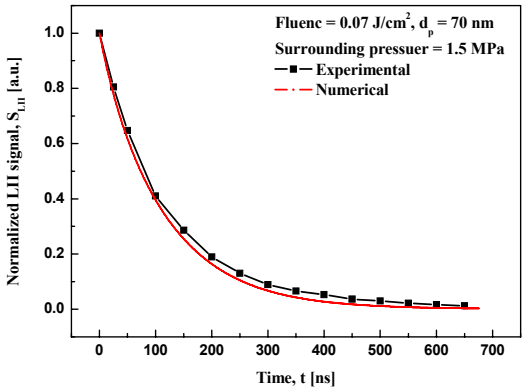

Fig. 11. Comparison of normalized LII signals at 1.5 MPa.

dicted result of 70 nm particle size based on decay time by determined numerical results. As can be seen in Fig. 11, it could confirm two signals were well matched and it is also confirmed that there will be a possibility to decide particle size to apply TIRE-LII at partially high pressure conditions through the results.

5. Conclusions

From the comparison of the results - vaporization, conduction, radiation, LII signal, soot particle temperature, change of primary particles size, decay time which are obtained from numerical calculation and an experiment under elevated surrounding pressure conditions, the following is concluded:

(1) The most dominant factor among vaporization, conduction and thermal radiation in heat transfer mechanism at elevated surrounding pressure up to 2.0 MPa is investigated. As surrounding pressure increases, conduction is the most dominant factor in the heat transfer mechanism in the cooling process of heated particles.

(2) From the heat transfer mechanism of the numerical result of LII, it is clear that the starting time of dominant heat conduction is shortened. So the accuracy of model could be enhanced by selecting an earlier signal in the decision of signal ratio while the TIRE-LII model is applied to higher surrounding pressure condition.

(3) Signal decay steeper and lifetime of signal is shortened as surrounding pressure increases in each result. Decay time relatively linearly increases as particle size increases, but it decreases as surrounding pressure increases in each result. And these parameters are matched well in comparison.

(4) The lifetime of LII signal is decreased as the elevated pressure is increased, so that LII decay time is also decreased in both results. As consequence, the LII numerical model in this study could be applied to decide particle size in TIRE-LII at the high pressure condition.

Acknowledgments

This work is funded by the Second Stage of Brain Korea 21 and Pusan Clean Coal Center(PC3) Research Grant and we are grateful for their financial support.

Nomenclature

Item	:	Description Unit
c_1	:	First constant in Planck's formula[W m^2]
c_2	:	Second constant in Planck's formula [W m^2]
c_s	:	Specific heat of soot [J kg^{-1} K^{-1}]
G	:	Heat transfer geometry factor for spheres
h	:	Heat transfer coefficient [W m^{-1} K^{-1}]
ΔH	:	Enthalpy of vaporization [J mol^{-1}]
I_L	:	Laser intensity [W m^{-2}]
k_∞	:	Thermal conductivity [W m^{-1} K]
m_p	:	Mass of a single of soot particle [kg]
n_∞	:	Refractive index of surrounding gas
P_v	:	Vaporized pressure of soot [N m^{-2}]
p^*	:	Vaporization pressure of soot [N m^{-2}]
$\dot{q}_{rad}$	:	Radiation energy [W m^{-2}]
$R(\lambda)$	:	Combined spectral response function
$r(t)$	:	Soot particle radius [m]
$T(t)$	:	Soot particle temperature [K]
T_∞	:	Surrounding temperature [K]
T^*	:	Vaporization temperature of soot [K]
W_v	:	Molecular weight of soot [kg mol^{-1}]
U_v	:	Langmuir evaporation rate [m/s]
α_{abs}	:	Absorption coefficient
λ	:	Detection Wavelength [m]
λ_{mpf}	:	Mean free path of vaporized particle in gas [m]
ρ_v	:	Density of vaporized soot [kg m^{-3}]
ρ_s	:	Density of soot [kg m^{-3}]

References

[1] R. R. Dickerson, S. Kondragunta, G. L. Stenchikov, K. L. Civerolo, B. G. Doddridge and B. N. Holben, The Impact of Aerosols on Solar UV Radiation and Photochemical Smog, http://metosrv2.umd.edu/aerosol.html, (1997).

[2] T. Lehre, B. Jungfleisch, R. Suntz and H. Bockhorn, Size Ditribution of Nanoscaled Particles and Gas Temperatures from Time-Resolved Laser-Induced-Incandescence Measurements, *Applied Optics,* 42, (2003) 2021-2030.

[3] R. W. Weeks and W. W. Duley, Aerosol-Particle Sizes from Light Emission during Excitation by TEA CO_2 Laser Pulse, *Journal of Applied Physics,* 45 (1974) 4661-4662.

[4] A. C. Eckbreth, Effects of Laser-Modulated Particle Incandescence on Raman Scattering Diagnostics, *Journal of Applied Physics,* 48 (1977) 4473-4479.

[5] L. A. Melton, Soot Diagnostics based on Laser Heating, *Applied Optics,* 23 (13) (1984) 2201-2208.

[6] C. J. Dasch, Continuous-Wave Probe Laser Investigation of Laser Vaporization of Small Soot Particles in a Flame, *Applied Optics,* 23 (1984) 2209-2215.

[7] B. Quey, T. W. Lee, T. Ni and R. Santaro, Spatially Resolved Measurement of Soot Volume Fraction Using LII, *Combustion and Flame,* 97 (1994) 384-392.

[8] S. Will, S. Schraml and A. Leipertz, Two-Dimensional Soot Particle Sizing by Time-Resolved Laser-Induced Incandescence, *Optics Letters,* 20 (22) (1995) 2342-2344.

[9] M. Hofmann, W. G. Bessler, C. S. Schulz and H. Jander, Laser-Induced Incandescence for Soot Diagnostics at High Pressure, *Applied Optics,* 42 (12) (2003) 2052-2062.

[10] C. Schultz, B. F. Kock, M. Hofmann, H. Michelsen, S. Will, B. Bougie, R. Suntz and G. Smallwood, Laser-Induced Incandescence: Recent Trends and Current Questions, *Applied Physics, B* 83 (2006) 333-354.

[11] H. Bladh, Characteristics of Laser-Induced Incandescence from Soot in Studies of a Time-Dependent Heat and Mass Transfer, *Applied Physics, B* 78 (2004) 241-248.

[12] T. Schittkowski, B. Mewes and D. Brüggemann, Laser-Induced Incandescence and Raman Measurements in Sooting Methane and Ethylene Flame, *PCCP,* (2002) 2063-2071.

[13] H. R. Leider, O. H. Krikorian and D. A. Young, Thermodynamic Properties of Carbon Up to the Critical Point, *Carbon,* 11 (1973) 555-563.

[14] B. J. McCoy and C. Y.Cha, Transport Phenomena in the Rarefied Gas Transition Regime**,** *Chemical Engineering Science,* 29 (2) (1974) 381-388.

[15] F. M. White, Viscous Fluid Flow, McGraw-Hill, New York, USA. (1991).

[16] L. E. Fried and W. M. Howard, Explicit Gibbs Free Energy Equation of State Applied to the Carbon Phase Diagram, *Physical Review, B* 61 (1999) 8734-8743.

[17] S. Will, S. Schraml and A. Leipertz, Comprehensive Two-Dimensional Soot Diagnostics Based on Laser-Induced Incandescence (LII), *Twenty-Sixth Symposium on Combustion*, (1996) 2277-2284.

[18] J. H. Lee, J. Y. Kim, D. S. Jeong, C. H. Jeon and Y. J. Chang, Numerical Investigation on Soot Primary Particle Size using Time Resolved Laser Induced Incandescence (TIRE-LII), *Transaction of the Korean Society of Mechanical Engineers,* B 29 (9) (2005) 1022-1031.

[19] G. B. Kim, S. W. Cho, J. H. Lee, D. S. Jeong, C. H. Jeon and Y. J. Chang, Study on Soot Primary Particle Size Measurement in Ethylene Diffusion Flame by Time-Resolved Laser-Induced Incandescence, *Transaction of the Korean Society of Mechanical Engineers,* B 30 (10) (2006) 973-981.